FISEVIER

Contents lists available at ScienceDirect

Case Studies in Thermal Engineering

journal homepage: www.elsevier.com/locate/csite





Experimental analysis on the effect of multi-level array hollow semi-stadium fins (HSSF) and baffles on solar thermal air collector

Muhammad Aqil Afham Rahmat ^{a,b}, Adnan Ibrahim ^{a,*}, Khaled M. Al-Aribe ^c, Muhammad Ubaidah Syafiq Bin Mustaffa ^a, Ihsan Okta Harmailil ^a, Sahibzada Imad Ud Din ^a

- ^a Solar Energy Research Institute, Universiti Kebangsaan Malaysia, 43600, Bangi, Selangor, Malaysia
- ^b Department of Biological and Agricultural Engineering, Faculty of Engineering, Universiti Putra Malaysia, 43400, UPM Serdang, Selangor, Malaysia
- ^c Department of Mechanical Engineering, Abu Dhabi University, 55911, Abu Dhabi, United Arab Emirates

ARTICLE INFO

Keywords: Solar thermal Fins Baffles Double-pass solar air collector Performance analysis Energy

ABSTRACT

An energy crisis is caused by the world's population expansion and growing energy consumption by global civilization, which encourages the usage of renewable energy technologies such as solar thermal collectors. Inefficient heat transmission lowers energy conversion and collector performance. This research aims to utilize a multi-level array of hollow semi-stadium fins (HSSF) with baffles to evaluate experimentally the double-pass solar air collector energy utilization. The proposed collectors with baffles and 1:2 and 1:4 multi-level spacing gaps are compared to the flat plate design at mass flow rates of 0.01-0.08 kg/s and irradiances of 400-800 W/m². The experimental findings are verified with numerical and previously experimental studies. The findings indicated that the newly double-pass solar collector achieved a maximum thermal efficiency of 77.70 % at 800 W/m2, the highest useful energy of 934.83 Watts, and the highest enhancement efficiency of 30.67 %, indicating better performance than the flat plate design. Optimal efficiency was found at flow rates of 0.04 kg/s (400 W/m²) and 0.07 kg/s (600–800 W/ m²). Increasing mass flow rates reduces friction factors while raising pressure drops. Validation with numerical results contains a 0.67-4.96 % error. Field-based experimental research, exergy and thermohydraulic studies, and economic and environmental studies are recommended to evaluate the design's effectiveness and feasibility.

Nomenclature

	Outlet temperature
T_o	
T_i	Inlet temperature
T_b	Bending temperature
T_{pm}	Mean plate temperature
m	Mass flow rate
C_p	Specific heat capacity
	(continued on next page)

(continued on next page)

E-mail address: iadnan@ukm.edu.my (A. Ibrahim).

https://doi.org/10.1016/j.csite.2025.106165

Received 2 January 2025; Received in revised form 24 March 2025; Accepted 17 April 2025 Available online 17 April 2025

2214-157X/© 2025 The Authors. Published by Elsevier Ltd. This is an open access article under the CC BY license (http://creativecommons.org/licenses/by/4.0/).

^{*} Corresponding author.

(continued)

	Outlet temperature
T_o	
Q	Useful energy
W	Watts
A_c	Collector's area
	Solar irradiation
U_t	Top loss
U_b	Bottom loss
U_{loss}	Total heat loss
h_{w}	Wind heat transfer coefficient
p	Density of air
T_{q}	Ambient temperature
k	Thermal conductivity of the insulation material
\mathcal{L}_d	Length of the duct
-u L	Thickness of the insulating material
D_h	Hydraulic diameter
- '' K _{fluid}	Thermal conductivity of fluid
Re Nu	Reynolds number
	Nusselt number
h	Heat transfer convective coefficient
w	Width of the duct
d	Height of the duct
f	Friction factor
V	Fluid velocity
W_B	Width of the baffle
L_B	Length of the baffle
⊏B Greek symbols	Length of the barne
η _{th}	Thermal efficiency
5	Stefan-Boltzmann constant
Sp.	Emittance plate
F G	Emittance of glass
β	Collector tilt angle
Abbreviations	
HSSF	Hollow semi-stadium fins
DPSAC	Double-pass solar air collector
SPAC	Single-pass solar air collector
TPSAC	Triple-pass solar air collector
FPSC	Flat plate solar collector
IEA	International Energy Agency
STSs	Solar thermal systems
SDG	Sustainable Development Goals
	International Air Transport Association
IATA	

1. Introduction

The global society is now experiencing an energy crisis as a result of the world's population growth and the rising need for energy in numerous industries such as heating, transportation and electricity. Furthermore, global energy consumption is predicted to climb by 33 % in 2040 [1,2]. The primary energy sources are fossil fuels, including coal, gas, and oil. However, their supply is restricted, and there is a likelihood that carbon dioxide emissions will negatively impact the global climate [3] Due to that, solar energy has the ability to provide an endless supply of energy as it is a renewable resource, thereby reducing environmental damage and emissions when fulfilling energy requirements [4–6]. According to the International Energy Agency (IEA), burning fossil fuels currently makes up around 80 % of global energy consumption. This trend is expected to continue, with a projected annual increase of 0.9 % until 2030. Conversely, renewable energy sources are expanding at a rapid pace, with an estimated annual growth rate of 3.0 % through 2030 [7–9].

Solar thermal systems, often known as STSs, are an alternative power supply known as a renewable energy source that helps to reduce the consumption of fossil fuels and the impact of pollution on the environment [10] The flat plate solar collector (FPSC) is one of the technologies employed in the solar thermal field to convert solar energy into heat energy. The collector designs can have many air channels. There are three configurations of solar air collectors based on the application: single-pass solar air collector (SPSAC), double-pass solar air collector (DPSAC), and triple-pass solar air collector (TPSAC) [11]. The solar air collector is applicable for drying purposes [12–14], and heating spaces [15–17], as reviewed by Fudholi et al. [18], indicating that the energy and exergy efficiencies of the solar air flat plate collector in this context range from 28 % to 62 % and from 30 % to 57 %, respectively. Additionally, the collectors can be implemented for water heating applications, as reviewed by Azha et al. [19].

Double-pass solar air collectors (DPSACs) can be made effectively by using several strategies [20,21] Implementing solar thermal air collectors is an initiative to achieve the Sustainable Development Goal (SDG) [10]. The Sustainable Development Goals (SDGs), organized by the United Nations, underline the importance of environmentally sustainable, cost-effective, and renewable energy

sources [22]. Since solar thermal technology development is crucial to creating cheap, sustainable, and clean energy, it aligns with the SDGs. The assessment conducted by Obaideen et al. [23] revealed that 72 % of the papers pertaining to solar energy technologies are included in SDG 7: Affordable and Clean Energy. Additionally, integrating solar energy has become crucial to achieving a sustainable and net-zero future [24] The IATA and ICAO-approved net-zero future 2050 [25] able an inexpensive energy supply, universal energy access, and sustained economic development [26].

The flexibility, simplicity, and cost-effectiveness of DPSAC make them a popular choice for solar energy applications. However, inefficient heat transmission [27] between the absorber plate and the airflow is the underlying problem with DPSAC, leading to significant thermal loss to the environment. The capability of the collector to acquire energy can be diminished due to inefficient heat transmission. Aside from that, flat-plate solar air collectors have poor efficiency due to the low convective heat transfer coefficient between the absorber plate and the moving air [28]. Increased absorber plate temperature accelerates thermal loss to the ambient in such collectors, particularly in natural convection. Due to the reduced collector flow rate, the absorber plate temperature of the collector is greater, lowering thermal efficiency. This issue has the potential to jeopardize DPSAC utilization in a variety of sectors. Due to that, using fins and baffles in the DPSAC can enhance its energy performance [29,30].

Several studies have been conducted on using fins and baffles in solar air collectors. Biswas et al. [31] discovered that cross-flow designs with 30-degree baffle angles had the highest thermal efficiency of 76.16 % due to improved airflow distribution and reduced pressure drop compared to channel and twist designs. According to the research, fins and baffles increase surface area and fluid retention time, improving solar collector thermal performance and efficiency. Findings from the study by Chabane et al. [32] showed that solar air heaters with rectangular baffle fins perform much better than those with smooth plates. At 80 m³/h flow rate and 34.8° tilt angle, the maximum efficiency reached was 58 %. This improvement was compared to the absorber plate configuration, where the baffle was positioned above the plate. Chand et al. [30] have shown that including louvred fins substantially improves the thermal productivity of solar air collectors. The louvred fins enhance airflow dynamics and increase the heat transfer area, resulting in

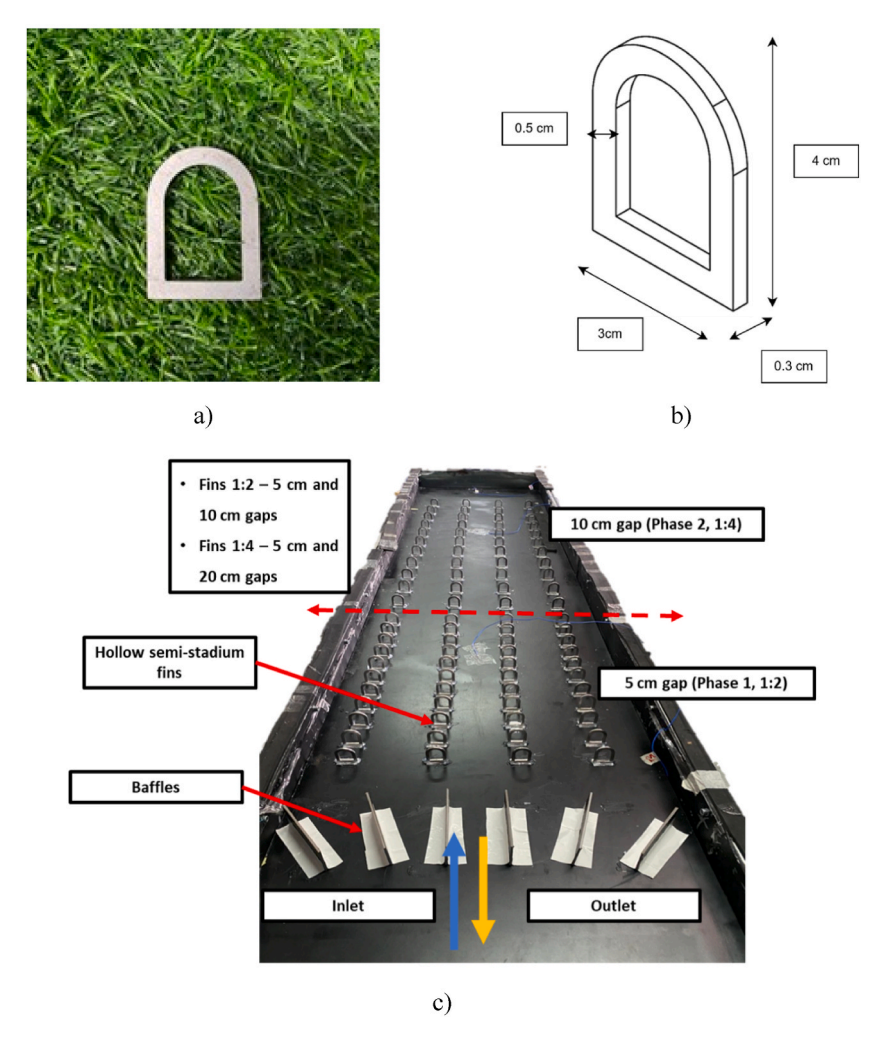


Fig. 1. Overview of multi-level array HSSF. a) Hollow semi-stadium fins (HSSF), b) Fins structure and dimensions, and c) Fins configuration in multi-level array with baffles at the absorber plate.

improved heat absorption and reduced thermal losses, which leads to higher outlet temperatures and overall efficiency. Given previous research, it is clear that fins and baffles substantially influence solar air collectors.

Energy analysis is necessary to determine the most efficient solar air collector [33]. Prior research on solar thermal collectors with an emphasis on energy evaluation has been conducted by a number of experts using various strategies. Azeez et al. [34] conducted an experimental study on a novel solar collector design that incorporates silicon carbide (SiC) nanofluids and phase change materials (PCM). The study achieved a maximum electrical efficiency of 11.7 % with a thermal energy efficiency of 87.7 %. Under optimal conditions, emphasizing the considerable influence of mass flow rates and solar irradiance on energy performance. In Morocco, Laasri et al. [35] demonstrated that the enhanced solar water heating system, which includes thermal energy storage and fins, has the potential to improve the energy efficiency of domestic hot water systems significantly. The energy savings achieved by the system range from 55.6 % to 63.2 %, depending on the climatic conditions. Poonam Rani and P.P. Tripathy [36] discovered that the semicircular loop of a single-pass solar collector obtained a considerable average energy efficiency improvement, with values reaching up to 76.60 % at an air mass flow rate of 0.02 kg/s, as opposed to lower efficiencies reported at lesser flow rates. Despite recent advances in solar thermal technology, there is still a significant gap in investigating the effects of hollow unique fin shapes with multi-level spacing gap configurations in double-pass solar thermal air collectors, particularly under varying flow rates and irradiance conditions. Therefore, this emphasizes the necessity of conducting further research in this area.

The primary objective of this study is to examine the energy performance of the double-pass solar air collector by employing a multi-level array configuration of hollow semi-stadium fins (HSSF) with baffles. In order to investigate the effectiveness of this

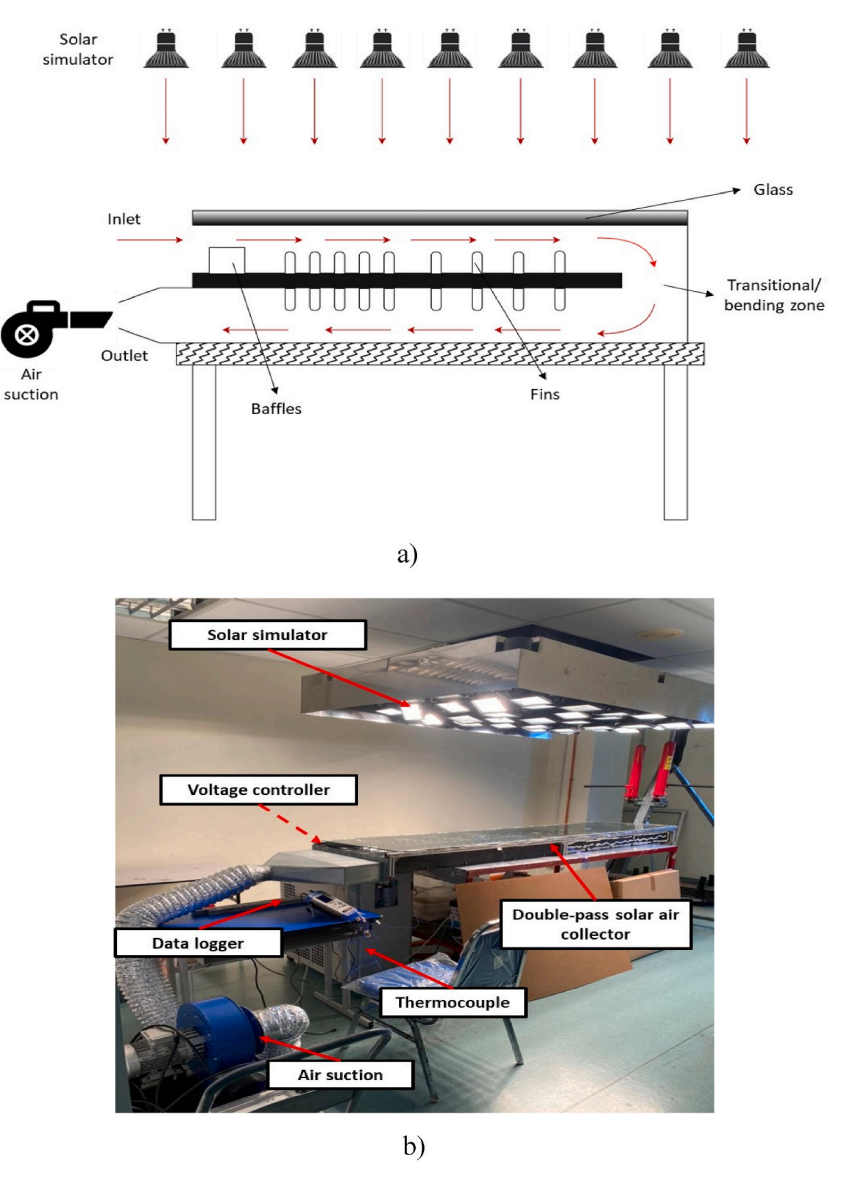


Fig. 2. a) Schematic view of the experimental setup, b) Indoor experimental setup.

collector, a thorough energy analysis is implemented. The novelty of this study is that the hollow fin with a semi-stadium design in the multi-level array arrangement has been implemented in the collector solar absorber. This investigation is an extended and experimental investigation that is predicated on the literature. The contributions described in this investigation include:

- A double-pass solar air collector with a multi-level spacing gap of HSSF and baffles can enhance the heat transfer effectiveness and improve the collector's airflow distribution, maximizing the collector's energy conversion.
- Different configurations between baffles and fins with varied spacing gaps (ratios of 1:2 and 1:4) are used to optimize the design and performance of the collector.
- Validation of the accuracy of the results is accomplished by comparing the performance between the experimental and numerical
 results. Additionally, studies from the past are compared to evaluate the effectiveness of the proposed design compared to other
 designs.
- A comprehensive performance analysis is focused on the thermal efficiency, thermal energy gained and losses, the temperatures
 across the collectors, and the fluid flow performance.

2. Methodology

2.1. New fins design description

Fins are very effective in enhancing the collector's thermal performance [11,30]. This study's solar thermal air collector incorporates novel stainless steel fins with a hollow semi-stadium shape arranged in a multi-level gap array. The fins have a unique shape that forms a semi-stadium shape, as shown in Fig. 1a) and 1b), which show the picture of the hollow semi-stadium fins (HSSF), including the dimensions and Fig. 1(c)) shows the multi-level arrangement.

A ratio of 1:2 is included in the multi-level gap, which allows for roughly equal air distribution and enhanced thermal performance. Phases 1 and 2 are separated by gaps of 5 cm and 10 cm (ratio 1:2), respectively. Furthermore, the fins are put on the collector's top and backplates as a double-sided setup to ensure the double-pass flow arrangement is used efficiently. In this research, several other configurations with ratios of 1:4 (5 cm and 20 cm gap) and various configurations are considered to evaluate the effect of gap ratios on thermal and fluid performance. The fin is optimized with previous studies suggested optimizing design characteristics of the fin to improve air distribution and thermal performance [37,38]. These fins have a height of 4 cm, a width of 3 cm, a fin thickness of 0.3 cm, and a hollow thickness of 0.5 cm.

2.2. Experimental test rig

Double-pass solar collectors are comprised of upper and lower ducts that facilitate the passage of airflow. The upper duct is between the glass cover and the solar absorber, connected to the HSSF and baffles. In contrast, the lower duct is situated between the bottom frame of the collector and the absorber plate affixed to HSSF and is in the opposite airflow direction. The transitional zone connects the upper duct to the lower duct, which is identified as a bending U-shape. Baffles and HSSF are employed in this experiment in various configurations to enhance the collector's performance. The collector's solar absorber is 2.3 m in length and 0.54 m in width, with a

Table 1Collector design parameters and experimental parameters of solar thermal collector.

Test rig parts	Parameters	Values	
Collector	Width \times length \times height, cm	54 x 230 x 17	
Glass cover	Emittance	0.85	
Absorber plate	Emittance	0.20	
Air Suction	Compressor capacity, kW	0.75	
Fins	Height, cm	4	
	Width, cm	3	
	Length, cm	0.3	
	Hollow thickness, cm	0.5	
Baffles	Height, cm	5	
	Width, cm	10	
Thermal insulation	Thermal conductivity, W/Mk	0.0262	
	Thickness, cm	4	
Experimental parameters			
Parameters	Values		
Irradiance, W/m ²	400–800		
Mass flow rate, kg/s	0.01-0.08		
Specific capacity of air C_p , J/kgK	1006		
Density of air, kg/m ³	1.225		
Wind heat transfer coefficient (h_w) ,	20–100		

thickness of 3.5 mm of black-painted aluminum. The upper channel depth is 0.063 m for the upper duct and 0.07 m for the lower depth. The duct's sides and bottom have been insulated with 2.5 cm and 4 cm thick softwood, respectively. Fig. 2(a) illustrates the experimental setup's schematic view.

The experimental test rig of DPSAC with HSSF and baffles is illustrated in Fig. 2(b). Aside from that, the glass cover has a thickness of 4.3 mm and is situated at the top of the upper duct, leaving a 0.063m gap between the absorber plate. The galvanized iron (GI) conduit connects the air suction with a capacity of 0.75 kW at the outlet section's conclusion, as illustrated in Fig. 2(b). The solar simulator and collector are separated by 1.5 m. Table 1 summarizes the design parameters for the double-pass solar air collector.

2.3. Experimental procedure

This test rig has three primary components: an air compressor, a solar simulator, and a new double-pass solar collector. The solar simulator and a compressor were employed to conduct this experiment indoors. Multiple researchers [39–41] conducted a study that determined that the use of tungsten halide lamps in the solar simulator was both reliable and adequate for the testing of indoor collectors by the minimal aspects or criteria outlined in ASHRAE standards. The indoor solar simulator in this investigation employs 30 tungsten halogen lamps with a maximal power consumption of 3000 W. A tungsten halogen lamp is a high-temperature incandescent light source that is compact and has a tungsten filament and halogen gas. It is ideal for applications such as solar simulators and projectors due to its high brightness, efficiency, continuous spectrum, longer lifespan, and UV emission. The LEDs are positioned at 1000 mm perpendicular to the upper cover of the DPSAH. The solar intensity received by the test heater was regulated by voltage controllers, each of which had a unit capability of 1000 VA. The solar mapping shows a non-uniformity of 6 % at 600 W/m² and 7 % at 800 W/m², classifying it as Class C based on uniformity standards [42]. Temperature measurements from the DPSAC are measured using a type K thermocouple. Due to its wide temperature range and great precision, the present study used the K-type thermocouple for thermal measurements. Similar experiments on solar thermal collectors have shown that K-type thermocouples are reliable for recording correct temperature data in the present investigation [43].

Numerous studies employ baffles and fins to experimentally investigate solar thermal collectors' efficiency. This research uses innovative fins and baffles to improve airflow to the collector. To optimize the design of DPSAC, five different configurations were investigated, from flat plate alone to HSSF and baffles with varying setups:

- 1. DPSAC plate with HSSF (multi-level gap 1:2) and baffles
- 2. DPSAC plate with HSSF (multi-level gap 1:2) only
- 3. DPSAC plate with HSSF (multi-level gap 1:4) and baffles
- 4. DPSAC plate with HSSF (multi-level gap 1:4) only
- 5. DPSAC flat plate

The experimental parameters were determined by a literature review, and ASHRAE solar thermal testing guidance. Then, each configuration was evaluated with various mass flow rates of 0.01–0.08 kg/s and irradiances ranging from 400 to 800 W/m². Table 1 lists the additional conditions used to derive the study's energy parameters and describes experimental conditions. The present configuration with HSSF outperforms conventional FPSC due to the improved thermal energy conversation caused by the enhanced absorber plate [11]. This modified absorber plate's increased surface area greatly increases the convective heat transfer coefficient between the air and the HSSF mounted to the absorber plate. This configuration can achieve the study's goal of thoroughly understanding the increase in thermal energy performance between the bare and proposed designs. The solar irradiance, mass flow rate, plate temperature, transitional zone temperature, and inlet/outlet temperatures are all measured. The average thermocouple readings are collected to calculate the temperature at each location. The study's result metrics include thermal efficiency, useable energy, energy loss, friction factor, and pressure drop for the double-pass FPSC. This research verified the findings by comparing them to numerical data gathered under identical conditions. Ansys Fluent software is used to provide numerical results. Furthermore, the data were compared to previous studies to determine consistency and identify differences.

2.4. Numerical setup

The thermal and flow dynamics of the designed solar air collector were simulated using Ansys Fluent software in the numerical setup. The numerical setup implies a uniform inlet air temperature of 24 $^{\circ}$ C, with solar irradiation varied at 400, 600, and 800 W/m² and mass flowrates ranging from 0.01 to 0.08 kg/s. The k- ϵ model was chosen as the turbulence model due to its ability to accurately predict flow characteristics in analogous applications, which enables the accurate prediction of fluid dynamics and heat transfer. The absorber plate, fins, and baffles have y + values ranging from 50 to 150, making them appropriate for standard wall functions. The experimental results were used to validate this model's accuracy, demonstrating its suitability for this form of thermal analysis. It is important to note that mesh independence analysis was achieved at the finer level, as the average element quality did not significantly improve with additional refinement. Consequently, the optimal selection was the finer mesh size with 3,340,851 elements, which achieved both accuracy and computational efficiency in the simulations.

2.5. Performance evaluation indicators

2.5.1. Thermal energy analysis

The solar air collector enables the direct conversion of solar radiation into thermal energy. Including fins and baffles could enhance the collector's energy performance [44]. This research investigates the energy performance of this novel collector by determining thermal efficiency, thermal energy acquisition, and loss. The solar collector's useable heat gain is calculated using solar irradiation and the observed values of the fluid's inlet temperature (T_i), outlet temperature (T_o), and fluid mass flow rate. Equation (1) below illustrates the useful heat gain [43,45].

$$Q_{ii} = \dot{m}C_{p_i}(T_0 - T_i) \tag{1}$$

The character C_p denotes the specific heat capacity of the fluid. The thermal efficiency of the collector can be calculated via Equation (2) [46,47].

$$\eta_{ib} = Q_{il} / A_c I$$
 (2)

While A_c represents the surface area of the collector, and I represents the solar irradiation.

Considerations such as the collector's design, insulation, operating temperature, and environmental conditions all contribute to energy loss in solar thermal air collectors, affecting the system's overall effectiveness. Flat plate solar collectors have a total heat loss coefficient that accounts for heat loss from the collector's top, back, and edge. The third term is presumed to be insignificant in this scenario according to the collector's standards. Heat loss from the top of the plate (U_t) and heat loss from the bottom (U_b) comprise the total heat loss coefficient. Equation (3) [45,48,49] state the parameters for the energy loss model.

$$Q_{loss} = U_{loss} A_c (T_0 - T_i)$$
(3)

Where U_{loss} is the collector's total heat loss coefficient. Equation (4) describes the heat loss coefficient.

$$U_{loss} = U_t + U_b \tag{4}$$

Where U_t and U_b are the top loss and backplate loss coefficients. The top loss coefficient formula is given by Equations (5)–(8).

$$U_{t} = \left[\frac{1}{\frac{C}{T_{p}} \left[\frac{(T_{p} - T_{a})}{(1+f)}\right]^{e}} + \frac{1}{h_{w}}\right]^{-1} + \frac{\sigma(T_{p} + T_{a})\left(T_{p}^{2} + T_{a}^{2}\right)}{\left(\varepsilon_{p} + 0/0059(1)h_{w}\right)^{-1} + \frac{1 + f + 0.133\varepsilon_{p}}{\varepsilon_{g}} - 1}$$
(5)

$$f = (1 + 0.089h_w - 0.1166h_w \varepsilon_p)(1 + 0.07866N)$$
(6)

$$C = 520(1 - 0.000051\beta^2)$$
 for $0^\circ < \beta < 70^\circ$; for $70^\circ < \beta < 90^\circ$, use $\beta = 70^\circ$ (7)

$$e = 0.430(1 - 100 / T_{pm})$$
 (8)

Where β is the angle of tilt of the collector. The bottom loss coefficient can be calculated using Equation (9).

$$U_b = \frac{k}{I} \tag{9}$$

Where L is the thickness of the insulating material and k is the thermal conductivity of the insulation material.

2.5.2. Fluid performance analysis

Friction factor and pressure drop are interrelated, substantially impacting the collector's energy performance. The Nusselt number is determined by Equation (10) [50].

$$Nu = \frac{h D_h}{k_{fluid}} \tag{10}$$

Where Dh is given by Equation (11).

$$D_{h} = \frac{4 (wd)}{2 (w+d)} \tag{11}$$

There is a connection between the friction factor and the pressure drop, which are both important characteristics. Equation (12) is used to determine the friction factor that acts inside the solar air collector [37].

$$f = \frac{2 D_h \Delta P}{L_d p v^2} \tag{12}$$

The collector's pressure losses are determined by calculating the pressure drop of the collector and the pressure at the bending zone. The case without fins and baffles is described as Equations (13)–(15) [51].

$$\Delta P_{\text{without fins and baffles}} = \Delta P_{\text{smooth}} + \Delta P_{\text{bend}}$$
 (13)

$$\Delta P_{\rm smooth} = 2\rho f V^2 L_d / D_h \tag{14}$$

$$\Delta P_{\text{bendiny}} = K_D V^2 / 2$$
 (15)

The pressure drop for the collector featuring fins and baffles is represented by Equation (15) and (16) [29].

$$\Delta P_{\text{fins and baffles}} = \left(1.465 \times 10^{-5}\right) Re_a^{1.94} \left(\frac{W_B}{D_h}\right)^{2.6} \left(\frac{L}{L_B}\right)^{1.2} + \frac{2fL_d V^2 \rho_a}{D_h}$$
(16)

Where f denotes the friction factor, p is the fluid density, V is the fluid velocity, and L_d is the duct length. The present system uses a value of 2.2 [51] for K for the 180° near reverse curve. The formula employed to validate the experimental and numerical tests is given in Equation (17) [30].

$$Percentage error = \frac{Numerical - experimental}{Experimental}$$
(17)

2.6. Governing equations

Equations and scientific principles called governing models explain fluid movement, heat transport, and related processes. These models often use energy, momentum, and mass conservation. The following equations describe the complex physical issue dynamics [52]. Equation (18) represents the continuity model. Equation (19) represents the momentum model. Equation (20) represents the energy model.

$$\frac{\partial \left(\rho_{hnf} U_{j}\right)}{\partial X_{i}} = 0 \tag{18}$$

$$\frac{\partial(\rho_{hnf} U_j)}{\partial X_j} = -\frac{1}{\rho_{hnf}} \frac{\partial p}{\partial X_i} + \frac{1}{\rho_{hnf}} \frac{\partial p}{\partial X_j} \left[\mu_{hnf} \left(\frac{\partial U_i}{\partial X_j} - \frac{\partial U_i}{\partial X_j} \right) - \rho_{hnf} \overline{u_i u_j} \right]$$

$$(19)$$

$$\rho_{hnf} U_j \frac{\partial T}{\partial X_i} - \rho_{hnf} \overline{T u_j}$$
 (20)

Additionally, Equation (21) shows heat fluxes in the energy expression, and Reynolds stresses in the momentum expression [52]. Equation (22) calculates turbulent viscosity μ_t . Equation (23) calculates turbulent dissipation.

$$\rho_{hnf} \, \overline{u_i u_j} = \mu_t \left(\frac{\partial U_i}{X_j} + \frac{\partial U_i}{\partial X_j} \right) + \frac{2}{3} \, \left(\rho k + \mu_t \, \frac{\partial U_i}{X_j} \right) \, \delta_{ij} \tag{21}$$

$$\mu_t \frac{\rho_{h\eta^K}}{\omega} \tag{22}$$

$$\omega = c_{\mu}^{\frac{3}{4}\frac{1}{K^2}} \tag{23}$$

The turbulence model constant is C_{μ} , and the turbulent length scale is t. The turbulence length scale in Equation (24) defines huge energy-containing eddies in turbulent flows. Heat flow is shown by $\overline{Tu_j}$, and Pr represents the turbulent Prandtl number. This study used the SST k- ω turbulence model for its high accuracy and efficiency. The preferred alternative was because the solar air collector in the study generates very turbulent flows [53]. The SST k- ω turbulence model represents turbulent flow kinetic energy as k and diffusing turbulence energy as ω . Equations (25) and (26) demonstrate this model [52,54].

$$\rho_{hnf} \, \overline{Tu'_j} = \frac{\mu_t}{Pr_t} \, \frac{\partial \overline{T}}{\partial X_i} \tag{24}$$

$$\frac{\partial(\rho_{hnf} kU_i)}{\partial X_i} = \frac{\partial}{\partial X_j} \left(r_{\omega} \frac{\partial k}{\partial X_j} \right) + G_k - Y_k + S_k \tag{25}$$

$$\frac{\partial \left(\rho_{hnf} \omega U_{i}\right)}{\partial X_{i}} = \frac{\partial}{\partial X_{i}} \left(r_{k} \frac{\partial \omega}{\partial X_{i}}\right) + G_{\omega} - Y_{\omega} + D_{\omega} + S_{\omega} \tag{26}$$

While G_k and G_ω represent the production of k and ω , respectively. The variable expansion of k and ω is represented by r_ω and r_k . Turbulence causes k and ω to dilate, represented by Y_k . D_ω refers to cross-diffusion, whereas S_k and S_ω reflect resource factors. Equation (27) (Discrete Ordinate) calculates radiant heat transfer using top-of-solar collector irradiances. The DPSAC's response to solar radiation was predicted using a discrete ordinate (DO) model. After [55] adding a volumetric source term S_h to Equation (28), the energy equation and radiative transfer computation are coupled:

$$\nabla \cdot \setminus \left(I_{\lambda} \left(\vec{r}, \vec{s} \right) + (\alpha_{\lambda} + \sigma_{s}) I_{\lambda} \left(\vec{r}, \vec{s} \right) = a n^{2} \frac{\sigma T^{4}}{\pi} + \frac{\sigma_{S}}{4\pi} \int_{0}^{4\pi} I(\vec{r}, \vec{s}) \phi(\vec{r}, \vec{s}) d\Omega \right)$$

$$(27)$$

$$S_h = -\frac{\partial q_{ri}}{\partial x_i} = \alpha \lambda \left(4\pi I_{b\lambda}(\vec{r}) - \int_{4\pi} I(\vec{r}, \vec{s}) d\Omega \right)$$
 (28)

2.7. Uncertainty analyses

Uncertainty analysis represents a systematic approach aimed at quantifying errors in estimations. The accuracy of measurements plays a crucial role in assessing the reliability and credibility of data. The uncertainty evaluation results for each piece of equipment are presented in Table 2. The analysis indicated that the uncertainties displayed values below 2 %, signifying enhanced measurement precision and reliability. The standard deviation s can be expressed using Equation (18) [43].

$$s = \sqrt{\frac{\sum_{i}^{n} (x_i - \overline{x})^2}{n - 1}} \tag{18}$$

The number of measurements, the mean of the measurements, and the results of the measurements are denoted as n, x_i and \overline{x} . Equation (19) represents the uncertainty, u.

$$u = \sqrt{\frac{s}{\sqrt{n}}} \tag{19}$$

3. Results and discussions

3.1. Relation of thermal energy efficiency and outlet temperature

Thermal energy efficiency, known as thermal efficiency, is one of the main parameters for assessing the energy performance of the solar air collector [56]. Outlet temperature is also a significant indicator since it can indicate if the system fits the intended application requirements [57] Fig. 3 shows the comparison between thermal efficiency and outlet temperature for DPSAC with HSSF (1:2 and 1:4) and baffles at variable mass flow rates (0.01–0.08 kg/s). The study was conducted at 400, 600, and 800 W/m² irradiance levels.

The impact of utilizing HSSF and baffles at a 400 W/m² irradiance level condition is illustrated in Fig. 3(a), which displays the relationship between these two parameters. The solar air collector's thermal efficiency was increased from a mass flow rate of 0.01 kg/s and reached optimum efficiency at a mass flow rate of 0.04 kg/s for all configurations. The efficiency exhibits minimal fluctuations at a mass flow rate of 0.04 kg/s and above. The DPSAC plate with HSSF (1:2) and baffles have the maximum thermal efficiency of 51.62 %, whereas the DPSAC flat plate shows the lowest efficiency at 34.98 %, both measured at a mass flow rate of 0.08 kg/s. The mass flow rate range for the DPSAC plate design with HSSF 1:2 and baffles is the biggest, spanning from 23.35 % to 51.62 %, while the DPSAC flat plate exhibits the lowest range, from 19.77 % to 34.98 %. In addition, the outflow temperature of all configurations decreased from a mass flow rate of 0.01 kg/s and began to exhibit negligible changes at a mass flow rate of 0.04 kg/s and higher. As a result, the maximum outlet temperature occurs at the lowest mass flow rate. In contrast, the lowest mass flow rate occurs at the highest mass flow rate under this irradiance scenario. Considering the average measurements across mass flow rates, the DPSAC plate with HSSF (1:2) -B and the DPSAC plate with HSSF (1:4) -B had a higher average outlet temperature of 31.75 °C and 32.68 °C, respectively. Meanwhile,

Table 2
Instrument uncertainties.

	Parameters	Model names	Measuring range	Units	Uncertainty values, %
Equipment					
Thermocouples	Temperature	Туре К	−200~1260 °C	°C	±0.1
Data logger	Temperature readings	AT4808 data taker	200~1300 °C	°C	± 0.1
Solar Power Meter	Irradiances	RS PRO	1999 W/m^2	W/m^2	± 1
Anemometer	Velocity of air	AM4206	0.4-25.0 m/s	m/s	± 1.2
Air Suction	Velocity of air	GTG GCIL 200	_	m/s	± 1.1

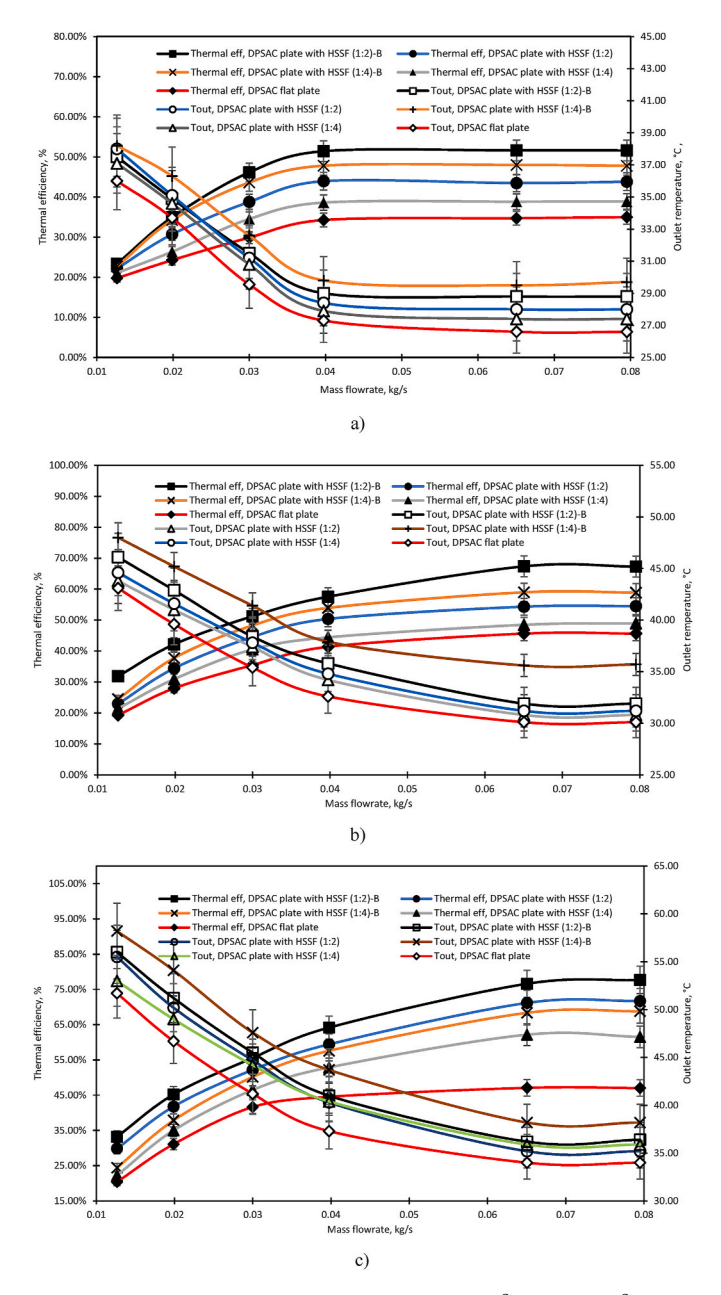


Fig. 3. Thermal efficiency and outlet temperature. a) 400W/m², b) 600W/m², c) 800 W/m.².

the DSPSAC flat plate has the lowest average outlet temperature, obtaining 29.96 $^{\circ}\text{C}.$

In comparison to the flat plate design with the proposed design in the optimum condition (0.04–0.08 kg/s), the DPSAC plate with HSSF (1:2)-B and plate with HSSF (1:4)-B has the greatest efficiency difference (16.90 % and 13.28 %). Meanwhile, the DPSAC plate with HSSF but without baffles had the lowest percentage efficiency discrepancies for both gap ratios 1:2 and 1:4, with 8.83 % and 3.90 %, respectively, at the optimum flow rates. This investigation demonstrates that the DPSAC with fins and baffles can offer significant enhancement compared to fins only. Regarding outlet temperature, the configuration DPSAC plate with HSSF (1:4)-B has the most significant outlet temperature rise of 3.10 $^{\circ}$ C compared to the flat plate design at the higher mass flow rates. The DPSAC plate with HSSF (1:2)-B exhibits the second most significant difference in output temperature at 2.2 $^{\circ}$ C. Collectively, it is proven that the performance of the collector is improved at irradiance of 400 W/m².

Fig. 3(b) presents a detailed comparison of thermal efficiency alongside outlet temperature under irradiance conditions at 600 W/m^2 . The graphs indicate that thermal efficiency for all configurations exhibited an increase beginning at a mass flow rate of 0.01 kg/s, ultimately achieving optimum efficiency at a mass flow rate of 0.07 kg/s and beyond. It also indicates that the DPSAC plate with HSSF (1:2)-B achieves the highest thermal efficiency of 67.37 % at a flow rate of 0.07 kg/s. The minimum efficiency recorded under optimal

conditions was approximately 48.94 % and 45.65 %, associated with the DPSAC utilizing HSSF (1:4) and the DPSAC flat plate configurations. The configuration of the DPSAC plate with HSSF 1:2-B exhibits the highest mass flow rate range, ranging from 31.88 % to 67.37 %. In contrast, the DPSAC flat plate shows the lowest range, between 19.28 % and 45.65 %.

Next, the trend of outlet temperature for all designs shows a decreasing pattern until it reaches negligible changes at a flow rate of 0.07 kg/s. As a result of that trend, the highest outlet temperature occurs at the lowest mass flow rate, whereas the lowest outlet temperature is observed at the highest mass flow rate. Based on the average readings across various mass flow rates, both the DPSAC plate with HSSF (1:2) -B and the DPSAC plate with HSSF (1:4) -B exhibit the highest average outlet temperature, calculated at 37.83 °C and 40.63 °C. Meanwhile, the DSPSAC flat plate only has the lowest average outlet temperature at 35.15 °C in this irradiance condition. The proposed configuration outperformed the flat plate design by 21.73 % and 13.34 %, respectively, at $600W/m^2$ for the DPSAC plate with HSSF (1:2)-B and HSSF (1:4)-B. Meanwhile, the lowest percentage efficiency difference was found for both DSPAC designs, with fins only contributing to 2.84 % and 8.87 %. This research shows that the DPSAC with fins and baffles can enhance substantially more than the flat plate alone. Regarding outlet temperature increment, the configuration DPSAC plate with HSSF (1:4)-B has the largest outlet temperature rise of 5.6 °C compared to the flat plate design for higher mass flow rates. Collectively, it is shown that the collector's performance improves with an irradiation of 600 W/m^2 .

According to Fig. 3(c), all designs' thermal efficiency increased from mass flow rates of 0.01 kg/s to the optimal flow rate of 0.07 kg/s at 800 W/m². At the optimal mass flow rate, the graph reveals that the efficiency of the DPSAC flat plate starts decreasing drastically while the DPSAC with a gap ratio of 1:4 exhibits just a slight efficiency reduction. In contrast, the DPSAC with a gap ratio of 1:2 maintains efficiency from flow rates of 0.07 kg/s forward. The maximum thermal efficiency was reached on the design DPSAC plate with HSSF (1:2)-B at 77.70 %, while the lowest efficiency at the optimal flow rate was on the design DPSAC flat plate at 47.09 %. Aside from that, the mass flow rates of the configuration of the DPSAC plate with HSSF 1:2 and baffles had the largest ranges from 33.21 % to 77.70 %, while the lowest ranges belonged to the DPSAC flat plate, ranging from 20.40 % to 47.09 %. In terms of the collector's output temperature, it decreases throughout mass flow rates until becoming stable at 0.07 kg/s onwards. In this irradiance situation, the greatest outlet temperature occurs at the lowest mass flow rate and the lowest at the highest rate. When averaged over mass flow rates, the DPSAC plate with HSSF (1:4) -B had the highest average outlet temperatures of 55.66 °C and 57.19 °C, respectively. Meanwhile, the DSPSAC flat plate has the lowest average outlet temperature, at 55.28 °C.

The efficiency difference between the proposed design and the flat plate design at 800 W/m2 and flow rates (0.07 kg/s - 0.08 kg/s) was 30.67 % for the DPSAC plate with HSSF (1:2) with baffles and 24.69 % without baffles. In contrast, the minimal percentage efficiency difference was recorded in HSSF (1:4), which achieved only 15.08 % at optimal flow rates. The analysis indicates that the DPSAC featuring multi-level array fins (1:2) demonstrates a significantly greater enhancement compared to fins (1:4) at this irradiance level. The configuration DPSAC plate with HSSF (1:4)-B exhibits the highest increase in outlet temperature, measuring 4.2 %, compared to the flat plate design at the maximum mass flow rate of 0.07 %. The data indicates that the collector's performance shows enhancement at an irradiance level of 800 %.

By summarizing the findings for all designs, the configuration with baffles and multi-level fins (1:2) outperforms the others. It has the maximum thermal efficiency at higher mass flow rates, implying improved heat transfer performance owing to enhanced turbulence. The design with flat plates has the lowest thermal efficiency, emphasizing the need for fins and baffles to improve performance. Fins with 1:4 spacing perform moderately, with designs with baffles slightly outperforming those without. Aside from that, configurations with a larger fin gap (1:4) often have higher outlet temperatures at greater flow rates, suggesting better temperature retention but lower heat transfer efficiency. The flat plate solar collector has the lowest temperature indicating a relatively weak heat transfer performance potential. Configurations with fins (1:2) and baffles had lower output temperatures than those with a larger fin gap (1:4), indicating greater heat transfer to the air at the price of temperature retention.

Most importantly, the efficiency trend across all designs and irradiance levels indicates that, at $400-800 \text{ W/m}^2$, efficiency became maximum after reaching the optimal mass flow rate. This analysis identifies the optimal performance design at an irradiance level of $400-800 \text{ W/m}^2$ for flow rates ranging from 0.01 kg/s to 0.08 kg/s, utilizing HSSF and baffles. The most significant enhancement effect observed was 30.67 % on the DSPAC plate HSSF (1:2)-B at the highest irradiance levels. However, with a further increase to 1000 W/m^2 , thermal efficiency is expected to decline owing to increased heat losses from radiation and convection, which become more pronounced at higher temperatures. Although efficiency initially increases with rising irradiance, the improvement rate decreases due to reduced efficiency in heat transmission and material constraints. The results of optimum efficiency and efficiency enhancement are

Table 3Summary of optimum thermal efficiency and efficiency improvement across irradiances.

Experimental sets	400 W/m ²		600 W/m^2		800 W/m ²	
	Optimum thermal efficiency,%	Enhancement effect,%	Optimum thermal efficiency,%	Enhancement effect,%	Optimum thermal efficiency,%	Enhancement effect,%
Plate 1:2 HSSF-	51.62	16.63	67.29	21.64	77.70	30.67
В						
Plate 1:2 HSSF	43.82	8.83	54.52	8.87	71.72	24.69
Plate 1:4 HSSF-	47.99	13.01	58.88	13.23	68.82	21.79
В						
Plate 1:4 HSSF	38.88	3.90	48.94	3.29	61.54	14.51
Flat plate	34.98	n/a	45.65	n/a	47.03	n/a

summarized in Table 3.

3.2. Relation of energy gained and losses

Energy gained is a useful energy [58] obtained by the solar air collector, while energy losses are the portions of incoming solar energy that do not contribute to beneficial heat transfer to the air passing through the collector. These losses result from the collector's thermal losses. These findings illustrate the enormous influence of multi-level fin arrays and baffles on the collector's energy gain and loss. The studies were performed at mass flow rates ranging from 0.01 kg/s to 0.08 kg/s, with 400, 600, and 800 W/m² irradiances.

At an irradiance of 400 W/m², as shown in Fig. 4(a), the energy gained for all designs exhibited an upward trend until it peaked at the optimal flow rate of 0.04 kg/s, beyond which the energy gained displayed minimal variation. The DPSAC plate HSSF (1:2)-B design achieves the maximum energy gain of 310.52 W at a mass flow rate of 0.08 kg/s. The minimum energy acquired, measured at 118.94 W, was associated with the DPSAC flat plate, observed at the lowest flow rate of 0.01 kg/s. The analysis of energy gain across various flow rates indicates that the collector design featuring fins (1:2) and baffles achieves the highest average useful energy, measuring approximately 259.81 W with baffles and 223.49 W without baffles. In the meantime, the fins ratio of 1:4 demonstrates an intermediate energy gain, averaging 244.89 W with baffles and 2198.83 W without baffles. The design of the flat plate collector exhibits the lowest average useful energy, approximately 178.35 W. The findings indicated that utilizing fins and baffles can enhance the energy output of the solar air collector.

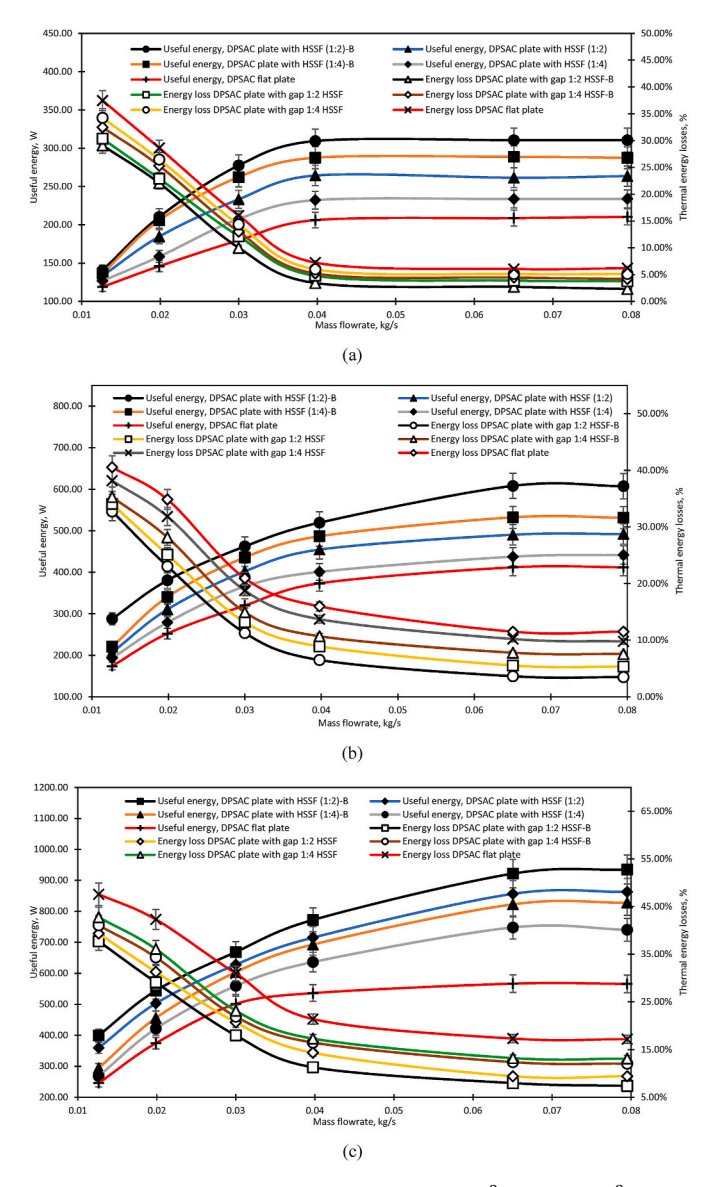


Fig. 4. Useful energy and thermal energy loss at a) 400 W/m², b) 600 W/m², c) 800 W/m.².

The analysis of energy losses across all designs indicates a discernible downward trend in the pattern of these losses. At a mass flow rate of 0.04 kg/s and beyond, the energy loss patterns for all designs begin to maintain a consistent level. Upon analyzing the energy losses at optimal flow rates, it is observed that the DPSAC flat plate exhibits the highest energy losses at 6.20 %, whereas the DPSAC plate HSSF (1:4 and 1:2)-B demonstrates the lowest energy losses at 2.72 % and 3.46 %. The findings indicate that the collector design featuring a multi-level fins ratio of 1:2 and 1:4, along with baffles, significantly minimizes energy losses at this irradiance level compared to alternative designs.

At an irradiance of 600 W/m², as shown in Fig. 4(b), the energy gained for all designs increased until it reached the optimal flow rate of 0.07 kg/s. At a flow rate of 0.07 kg/s and beyond, all designs exhibit minimal changes in useful energy. In addition, the design DPSAC plate HSSF (1:2)-B achieved the highest energy gain of 607.24 W at a mass flow rate of 0.08 kg/s, while the lowest energy gain of 174.02 W was recorded for the DPSAC flat plate at a flow rate of 0.01 kg/s. The energy gain pattern across flow rates indicates that the collector design with fins (1:2) achieves the highest average useful energy, approximately 477.50 W with baffles and 392.75 W without baffles. The fins ratio 1:4 yields intermediate energy gains of 424.51 W with baffles and 353.05 W without baffles. The design of the flat plate collector exhibits the lowest average useful energy, approximately 323.89 W. The findings indicated that incorporating fins and baffles enhances the energy output of the solar air collector.

Regarding energy losses, the pattern for all designs indicates a downward pattern. However, at a mass flow rate of 0.07 kg/s and beyond, the patterns of energy losses for all designs indicate a maintained pattern. When evaluating energy losses at optimal flow rates (0.07 kg/s) and beyond), the DPSAC flat plate has the maximum energy loss of 11.50 %. Compared, DPSAC plate HSSF (1:2) with baffles has the lowest energy losses at 3.64 %.

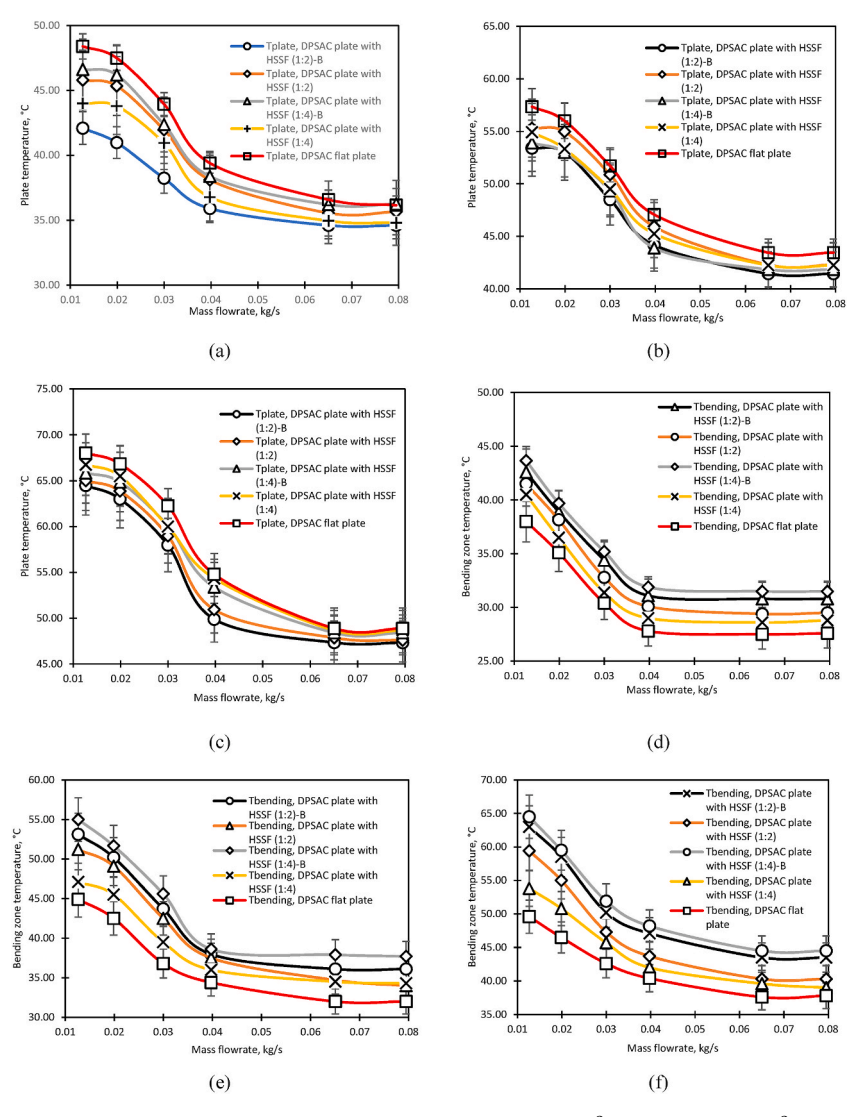


Fig. 5. Mean plate temperature and vending temperature of the collector. (a) T_{pm} at 400 W/m^2 , (b) T_{pm} at 600 W/m^2 , (c) T_{pm} at 800 W/m^2 , (d) T_b at 400 W/m^2 , (e) T_b at 600 W/m^2 , (f) T_b at 800 W/m^2 .

At an irradiance of 800 W/m2, as depicted in Fig. 4(c), the trend of energy gaining for all designs exhibited an increase until it attained the optimal flow rate of 0.07 kg/s, at which point the energy gained demonstrated a steady pattern. All configurations exhibit minimal changes from a flow rate of 0.07 kg/s onwards. The DPSAC plate HSSF (1:2)-B design achieves the highest energy gain of 934.83 W at a mass flow rate of 0.08 kg/s. The minimum energy acquired, quantified at 245.45 W, was attributed to the DPSAC flat plate operating at the minimal flow rate of 0.01 kg/s. The analysis of energy gain across varying flow rates indicates that the collector design featuring fins (1:2) achieves the highest average useful energy, approximately 706.84 W when baffles are included and 654.07 W in their absence. In the interim, the fins ratio 1:4 exhibits an intermediate energy gain, averaging 6161.11 W with baffles and 562.21 W without baffles. The design of the flat plate collector yields the lowest average useful energy, approximately 464.87 W. The findings indicated that incorporating fins and baffles can enhance the energy harvested by the solar air collector.

The pattern for all designs reveals a downward tendency in terms of energy losses. The maximal energy loss of 17.18 % is observed in the DPSAC flat plate when energy losses are assessed at optimal flow rates (0.07 kg/s and beyond). The DPSAC plate with HSSF (1:2)-B exhibits the lowest energy losses at 7.96 % in comparison. This research demonstrates that the flat plate design has a larger energy loss than the multi-level fins and baffles collector design for all irradiance levels.

3.3. Absorber plate and transitional zone temperatures

3.3.1. Absorber plate

Solar absorber plate temperature is one of the indicators used to measure the collector's thermal behavior. The plate temperature was calculated by obtaining an average reading of the absorber plate and recording it across various mass flow rates $(0.01-0.08 \, \text{kg/s})$ and irradiances $(400-800 \, \text{W/m2})$. These findings show the importance of fin spacing and baffles in determining the collector's thermal performance.

Fig. 5(a) presents the plate temperature behavior of a DPSAC subjected to an irradiance of 400 W/m², analyzing five different configurations. The design featuring flat plate fins (1:2) and baffles consistently results in the lowest plate temperature, leading to an average plate temperature of 37.74 °C. The DPSAC plate featuring HSSF (1:4)-B demonstrates intermediate performance, exhibiting average plate temperatures of 39.21 °C. This suggests that the wider fin spacing leads to a reduction in thermal performance when compared to the 1:2 configuration. The DPSAC flat plate configuration distinctly exhibits the highest average plate temperature at 42.00 °C, indicating a minor decrease in heat retention attributed to the lack of baffles and fins. This analysis indicates that the configuration with DPSAC plate HSSF (1:2)-B attained the lowest plate temperature of 34.60 °C at the optimal flow rate. In the meantime, the configuration DPSAC flat plate recorded the highest plate temperature of 36.58 °C at the optimal flow rate.

The plate temperature performance of DPSAC with five different configurations at 600 W/m2 irradiation is shown in Fig. 5(b). Among them, the DPSAC plate with HSSF (1:2)-B produced the lowest plate temperature, with an average of 47.00 °C. The DPSAC plate HSSF (1:4) with baffles has an average temperature of 47.30 °C. The DPSAC with a flat plate has the highest average plate temperature at 49.84 °C. Overall, at mass flow rates of 0.07 kg/s and above, the DSPAC flat plate has the highest plate temperature, while the DPSAC with fins 1:2 and 1:4 with baffles has the lowest plate temperature.

The plate temperature behavior for all configurations is shown in Fig. 5(c) at an irradiance of 800 W/m2. Plate temperatures decrease with increasing mass flow rate since greater flow rates promote convective cooling. However, with a mass flow rate of 0.07 kg/s onwards, the temperature shows an insignificant decrease. In terms of average readings, the DPSAC plate HSSF (1:2)-B has an average value of 55.66 °C, while the DPSAC flat plate has an average of 58.05 °C, giving them the highest average of the entire proposed designs. The solar air collector with a flat plate has the highest plate temperature, while the plate with multi-level fins (1:2) has the lowest plate temperature. This is due to the fact that the fins facilitate heat transfer, which effectively reduces the absorber plate temperature by more efficiently transferring heat to the air.

3.3.2. Bending zone

The transitional or bending zone temperature is critical to the collector's overall efficiency. The bending zone temperature is recorded for five proposed designs at a mass flow rate of 0.01-0.08 kg/s under irradiance levels of 400, 600, and 800 W/m². The results emphasize the temperature relationship at the U-bending section in Fig. 5 with the HSSF and baffles. At an irradiation of 400 W/m², as shown in Fig. 5(d), the bending temperature behavior decreases for all designs. The DSPAC plate design with HSSF (1:4)-B has the largest bending zone temperature range, with an average temperature of 35.58 °C, followed by HSSF (1:2)-B, which has the second highest average temperature of 34.77 °C. The lowest transitional zone temperature range occurred on the DPSAC flat plate, with an average measurement of 31.07 °C. In terms of the comparison at optimal mass flow rates (0.04 kg/s and above), the greatest bending area temperature was 31.50 °C (DPSAC with HSSF (1:4)-B), while the lowest temperature was 27.50 °C.

According to Fig. 5(e), at an irradiation of 600 W/m2, the transitional zone temperature trend declined across different flow rate values. In all five configurations, the DPSAC plate with HSSF (1:4)-B has the greatest average transitional zone temperature at 44.41 $^{\circ}$ C, suggesting a larger temperature variation across flow rates. Meanwhile, the DPSAC flat plate had the lowest average temperature at 37.10 $^{\circ}$ C, showing the lowest bending temperature range at this irradiance level. At the optimal flow rate (0.07 kg/s), the greatest temperature was 37.90 $^{\circ}$ C on DPSAC with a 1:4 multi-level fins ratio and baffles, while the lowest temperature was 32.00 $^{\circ}$ C on the flat plate collector. At an irradiance of 800 W/m2, as indicated in Fig. 5(f), the bending zone temperature trend decreased in relation to the flow rate. The temperature variations are minimal at a mass flow rate of 0.07 kg/s. The DPSAC plate with HSSF (1:2)-B exhibits the highest average temperature of 50.97 $^{\circ}$ C among all five configurations. The lowest average temperature recorded was 42.42 $^{\circ}$ C, indicating that the DPSAC flat plate resulted in a nearly 9 $^{\circ}$ C difference in bending temperature under these irradiance levels. The increased average temperature of the bending zone suggests that the bending zone temperature on the DPSAC with a fin gap of 1:2

and 1:4 is elevated relative to the flat plate design. Regarding the optimum flow rate starting from 0.07 kg/s at 800 W/m 2 , the maximum bending zone temperature recorded was 44.50 $^{\circ}$ C for the DPSAC flat plate at a flow rate of 0.07 kg/s. Conversely, the minimum temperature observed was 37.60 $^{\circ}$ C for the DPSAC plate with HSSF (1:4)-B at a flow rate of 0.08 kg/s. This examination illustrates the influence of transitional zone temperature on the solar collector employing HSSF and baffles.

3.4. Relation of friction factor and pressure drop

Pressure drop and friction factor are two critical variables in analyzing fluid flow performance, which can impact the general energy effectiveness of the system. Fig. 6(a) illustrates the relationship between pressure drop and friction factor for a double-pass solar air collector, including five proposed designs comprising flat plates and multi-level fins with baffles at gap ratios of 1:2 and 1:4. It underscores notable disparities in pressure drop and friction factor resulting from different designs. These findings include all irradiation levels for flow rates ranging from 0.01 kg/s to 0.08 kg/s since the variations in pressure drop and friction factor for each irradiance are minimal.

Based on Fig. 6(a), it is evident that the pressure loss for all designs has increased. Furthermore, the friction factor pattern for DPSAC with fins (ratio 1:2 and 1:4) deteriorated with increasing mass flow rates, but the DPSAC flat plate design remained consistent throughout flow rates. The configuration with gap 1:2 HSSF has the maximum pressure drop, roughly 17.44 Pa, at a mass flow rate of 0.08 kg/s, while the DPSAC with flat plate design has the lowest pressure drop, near 0.34 Pa, with a mass flow rate of 0.01 kg/s. In terms of optimum mass flow rates, the DPSAC plate HSSF (1:2) without baffles has a larger pressure drop of 17.44 Pa, compared to 17.25 Pa with baffles. For HSSF 1:4, the design without baffles has a larger pressure drop of 14.14 Pa than with baffles, which is 13.66 Pa. The friction factor parameter reaches its lowest around 0.03 at the highest flow rates for the DPSAC plate HSSF (1:4) with and without baffles, while the lowest (0.01) for the DPSAC flat plate design is similarly at the highest mass flow rates. The DPSAC plate with a 1:2 fin ratio obtained the lowest friction factor of 0.02 at the greatest flow rates. These variants show the effect of baffle and fin layouts on airflow resistance.

Analysis of the configurations reveals that the inclusion of fins and baffles significantly reduces the friction factor while simultaneously elevating the pressure drop across the flow rates owing to increased turbulence and flow resistance. The 1:2 HSSF-B configuration exhibits enhanced turbulence, leading to increased pressure drops while indicating improved thermal performance. Conversely, the flat plate has the lowest average friction factor and pressure drop, signifying minimum resistance and smooth airflow. The 1:4 HSSF configuration yields elevated pressure drop and friction factor values, although it exhibits diminished thermal performance, presenting a possible trade-off for optimizing thermal and hydraulic efficiency. Baffles are influenced by reducing the pressure drop of the solar collector. The graph highlights the trade-offs between thermal enhancement and the energy consumption necessary for airflow in the collector.

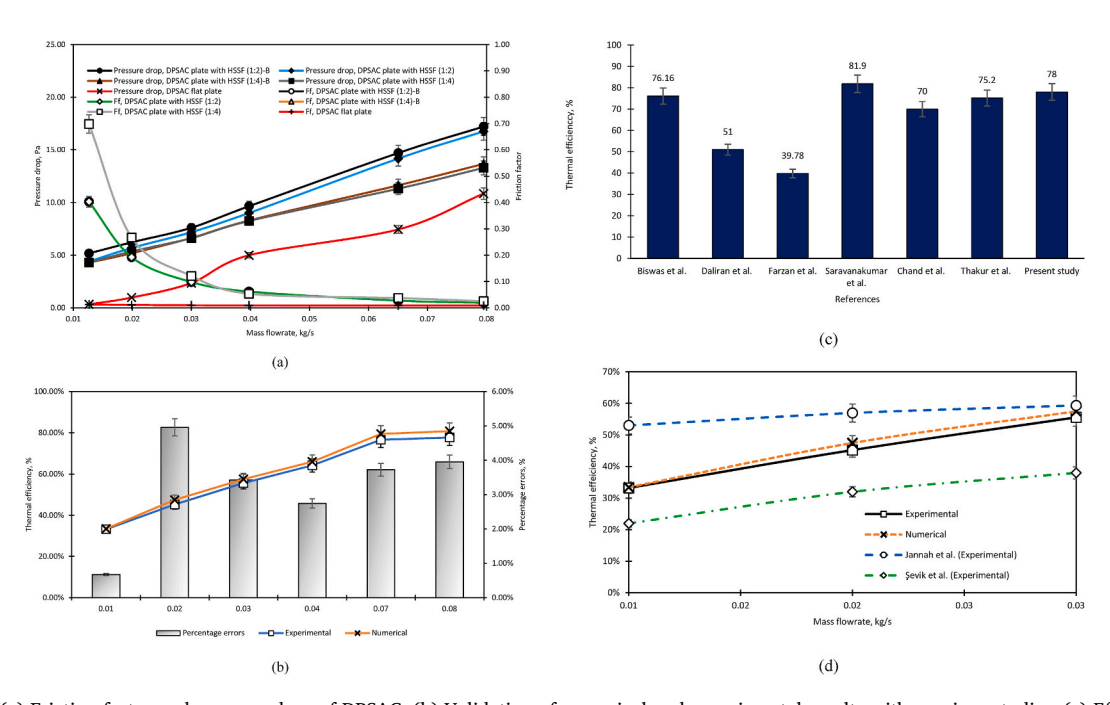


Fig. 6. (a) Friction factor and pressure drop of DPSAC, (b) Validation of numerical and experimental results with previous studies, (c) Efficiency comparison of the present study with past studies, (d) Comparison of experimental and numerical results of DPSAC with multi-level array HSSF and baffles at 800 W/m.².

3.5. Validation of experimental and numerical results

The experimental findings of DPSAC with multi-level HSSF and baffles were evaluated against numerical results using Ansys Fluent software. Similar mass flow rates from 0.1 to 0.3 kg/s and working fluid of air were used to determine the accuracy of the findings. Fig. 6(b) depicts the validation study between numerical and experimental studies of the most effective design (solar air collector with fins ratio 1:2 and baffles). Table 4, estimated a percentage error between the numerical and experimental data sets. It is evident that both outcomes exhibit an identical pattern, indicating that thermal efficiency increases as the mass flow rate increases. This pattern indicates that the experimental and numerical methods are in strong agreement, which validates the accuracy of the results. A small deviation is observed at lower flow rates, with a 0.67 % error, indicating that the numerical results slightly overestimate the thermal efficiency compared to experimental data. This discrepancy may be attributed to idealized assumptions in the numerical simulation, such as the neglect of losses. The disparity decreases as the flow rate increases, with a ranging error of 0.67–4.96 %. The curves come together at the maximal flow rate, confirming thermal efficiency in practical and predicted results. Overall, the numerical model accurately reflects the performance trends experimentally demonstrated.

The numerical findings were validated by comparing the results to those from previous experimental studies, as shown in Fig. 6(d). Compared to previous experimental research, the thermal efficiency achieved in this work surpasses that reported by Şevik et al. [59] due to using a flat-plate collector, which offers less heat transfer improvement. In contrast, Jannah et al. [60]'s findings show better thermal efficiency, which can be related to changes in the size and design of their double-pass solar air collector, which may alter heat retention and flow distribution.

4. Comparison with past studies

The effectiveness of the solar air collector using HSSF and baffles is compared with selected past studies, as seen in Fig. 6(c). Table 4 provides an overview of the enhancement efficiency between the proposed design and the reference solar collector design for each investigation, including the current study. The present study has demonstrated a superior performance, surpassing the majority of previous studies, as evidenced by Fig. 6(c). The present research achieved a thermal efficiency of 77.70 %, which surpassed that of Daliran et al. [62] at 51 %, Farzan et al. [62] at 39.78 %, and Thakur et al. at 75.2 %. Implementing multi-level semi-stadium fins and baffles in the solar air collector has substantially improved system performance. Furthermore, the baffles in the air collector improve air mingling and reduce dead zones, while the multi-level semi-stadium fins increase the surface area for heat transfer. The superior performance is likely attributable to this combination. As illustrated in Table 4, the present study exhibited an enhancement effect of 26 %, comparable to previous studies that reported an enhancement effect spanning from 21 to 34 %. It is important to note that thermal efficiencies have generally improved over time, with recent studies (2018–2024) demonstrating enhanced performance levels. It can be seen that the novel method in the utilization of hollow semi-stadium fins in a multi-level array configuration achieved a thermal efficiency of 77.70 %, which is significantly higher than the existing findings, which typically report efficiencies ranging from 58 % to 75.20 %. Consequently, this represents a significant improvement in the design of solar thermal collectors.

Table 5 provides a comprehensive overview of the performance of solar collectors as a result of various techniques that employ fins and baffles. The thermal efficiency of the collector can be improved by the implementation of a variety of fin and baffle designs [29–31]. Additionally, the effectiveness of the fluid is enhanced by the use of baffles and fins [61–63]. Moreover, this technique enhances the economic performance and drying performance of solar dryer systems [16,64,65]. The results of this research correspond with those of [29–31,61,63] who also indicated enhancements in thermal efficiency and useable energy via the utilization of fins and baffles, hence validating the observed trend's consistency. However, the results of this investigation provide a contradictory

Table 4Percentage error of experimental and numerical results as well as summary of past studies using fins and baffles.

Percentage errors					
Mass flow rate, kg/s	Irradiance W/m ²	Thermal efficiency, %	Percentage error, %		
		Numerical	Experimental		
0.01	800	33.43	33.21	0.67	
0.02		47.45	45.21	4.96	
0.03		56.48	55.58	3.42	
0.04		64.94	64.18	2.74	
0.07		79.46	76.61	3.72	
0.08		80.77	77.70	3.95	
Comparison of past studi	es				
Authors	Refs	Enhancement effect,%	Highest Thermal efficiency,%	Year	
Biswas et al.	[31]	34.20	76.16	2024	
Daliran et al.	[61]	21.00	51.00	2018	
Farzan et al.	[62]	25.78	39.78	2024	
Saravanakumar et al.	[29]	28.30	81.90	2019	
Chand et al.	[30]	32.00	70 0.00	2022	
Thakur et al.	[63]	_	75.20	2024	
Present study	_	30.67	77.70	_	

Table 5Enhancement techniques used from previous studies.

	Technique used	Impacts	Year
References			
Biswas et al. [31]	Using channel, cross flow, and twist fin designs on solar air collector	Increased the thermo-hydraulic performance of the solar collector by up to 25% performance enhancement	2024
Saravanakumar et al. [29]	Using arc-shaped rib roughened barrier with fins and baffles	Enhanced the energy and effective efficiency by 28.3 % and 27.1 %	2019
Chand et al. [30]	Utilizing louvered fins	The thermal performance is enhanced compared to a flat plate collector with an outlet temperature of 56 $^{\circ}\text{C}$ and 70 $\%$ efficiency	2022
Thakur et al. [63]	Applying V-shaped staggered baffles on the absorber plate	The optimization of the design enhanced the Nusselt number, which led to higher thermo-hydraulic performance by 3.67	2024
Daliran et al. [61]	Attaching fins at the bottom of the plate	Increased the Reynolds and Nusselt numbers by 16.23 and 5814.2, respectively.	2018
Farzan et al. [62]	Using perforated baffles as cooling solutions	Boosted the efficiency of the solar collector up to 39.78 % compared to without baffles	2024
Dutta et al. [16]	Using waste stone chips below the absorber plate of the solar dryer	Improved the exergy performance and economic performance with 69.13 % and 0.47 years payback period	2024
Dutta et al. [65]	Using corrugated solar absorber for natural convection solar dryer	Reduced the drying time by 27 h less, improved drying efficiency up to 10.77 %, and improved economic performance with 0.6 years payback period	2021
Kherrafi et al. [64] Present study	Using offset strip fins Using a hollow semi-stadium fin structure in a multi-level array arrangement combined with baffles	Increased economic efficiency by 33 $\%$ and 0.95 years payback period Enhanced thermal efficiency and achieved useful energy by up to 30.67 $\%$ and 934.83 W.	2023

conclusion compared to Daliran et al. [61]. The research indicated that fins could lower Reynold and Nusselt numbers at a constant mass flow rate, implying that variations in experimental conditions, material characteristics, or methodological methods may have influenced the results.

In terms of user-centric design analysis, the double-pass solar thermal air collector with baffles and multi-level hollow semi-stadium fins (HSSF) must take into account both technical performance and user needs. The results indicate that optimal flow rates can be customized to meet specific operational requirements, providing flexibility for a variety of user scenarios, particularly in industrial and agricultural drying applications. This emphasis on usability, in conjunction with a dedication to minimizing energy consumption and optimizing output, demonstrates a substantial advancement in user-centric design strategies that are intended to enhance the overall satisfaction and acceptance of solar thermal technologies among end users, in addition to enhancing technical performance.

While the study offers major advances in solar thermal collector technology using HSSF and baffles, it is critical to solve the real-world issues that could impede commercialization. The performance metrics were derived from regulated environments, which may not be universally applicable, and one of the prominent limitations is the reliance on specific climatic conditions. Another limitation is that this collector is exclusively appropriate for double-pass configurations and low-temperature applications due to the low-temperature range output. The challenges encountered were the production and material costs associated with assuring the durability and effectiveness of HSSF, and baffles can present additional obstacles to widespread adoption. The research also suggests the need for additional research into the cost-benefit analyses to ascertain the economic feasibility. Providing a more pragmatic perspective on the technology's pathways to commercialization, a comprehensive examination of potential market barriers, such as the present competition with conventional energy sources and the necessity of supportive policies and incentives, is possible.

5. Conclusion

The comprehensive evaluation of energy improvement employing multi-level array hollow semi-stadium fins (HSSF) and baffles in the solar air collector was investigated experimentally and verified using numerical findings and previous research. This research contributes to the thermal performance improvement of a double-pass solar air collector by integrating multi-level spaced HSSF fins and baffles, optimizing configurations with 1:2 and 1:4 gap ratios, validating experimental and numerical results, and providing a comprehensive analysis of thermal efficiency, temperature distribution, energy gains, energy losses, and fluid flow performance. The study's originality is the incorporation of a semi-stadium fin shape with a hollow feature in the fin's configuration of a multi-level array, which improves thermal energy performance in the collector and is beneficial for solar drying applications. The research examined the utilization of multi-level array HSSF at various multi-level ratios (1:2 and 1:4) in conjunction with baffles to create five sets of configurations, including a flat plate. The investigation was carried out with air mass flow rates ranging from 0.01 kg/s to 0.08 kg/s and irradiance values of 400–800 W/m². The assessment parameters include thermal efficiency, useful energy, energy losses, collector temperatures, friction factor, and pressure drop. This detailed energy study reveals that using multi-level array hollow semi-stadium fins (HSSF) and baffles in a solar air collector greatly improves overall collector performance, leading to the following conclusions:

- The main results indicated that the newly developed double-pass solar collector attained a maximum thermal efficiency of 77.70 % at 800 W/m², a peak useful energy output of 934.83 Watts, and a maximum enhancement efficiency of 30.67 %, signifying superior performance compared to the flat plate design.
- Besides that, the outcomes had shown that the optimal flow rates of 0.04 kg/s and onwards were attained at 400 W/m² solar irradiation, while flow rates of 0.07 kg/s and onwards were achieved at 600 and 800 W/m², implying minimal fluctuation and maximum efficiency.
- Other main results are shown where the efficiency improvement of the proposed designs over the flat plate design varies greatly via different irradiance levels (400–800 W/m². The double-pass solar air collector (DPSAC) with HSSF (1:2)-B and (1:4)-B achieves efficiency increases of 16.90 % and 13.28 %, respectively, at 400 W/m². The performance difference increases at 600 W/m², with the HSSF (1:2)-B configuration outperforming the flat plate by 21.73 % and the HSSF (1:4)-B by 13.34 %. At 800 W/m², the DPSAC with HSSF (1:2)-B outperforms the flat plate design by 30.67 %, demonstrating substantial effectiveness under higher irradiation conditions.
- The configuration with baffles and multi-level fins (1:2) outperforms the others. Its highest thermal efficiency (77.70 %) at higher mass flow rates (0.07 kg/s) indicates more excellent heat transfer due to turbulence. A larger fin gap (1:4) results in higher output temperatures (40.63 °C) at higher flow rates, indicating better temperature retention but worse heat transfer efficiency. Hollow fins with a semi-stadium structure and multi-level gap arrangement boost thermal energy gaining and collector energy efficiency. Baffling spreads air uniformly, which improves solar absorber heat energy absorption.
- The solar air collector can harvest the most energy using HSSF, and the baffles are 934.83 W at an optimal flow rate of 0.08 kg/s. Analysis of thermal energy losses at optimal flow rates shows that the flat plate design has the highest average thermal losses, reaching 29.00 % at 800 W/m². In contrast, the plate design with HSSF and baffles exhibits lower average thermal energy losses at higher irradiance levels, with 19 % and 23 %.
- The investigation indicates a bending zone and plate temperature decline as flow rates increase. The fins enhance heat transfer under elevated irradiance conditions, leading to a more significant reduction in the absorber plate temperature by optimizing the heat transfer to the air. The analysis indicates that incorporating fins and baffles leads to a notable reduction in the friction factor while also increasing the pressure drop across the flow rates due to raised turbulence and flowing resistance.
- The experimental and numerical results have been validated, showing a percentage error range of 0.67–4.96 %. The current investigation has also shown exceptional results, exceeding most earlier research efforts. The findings are also related to similar studies on solar air collectors that are designed for low-temperature applications and employ a double-pass configuration. The study's potential sources of error include measurement errors from devices such as thermocouples and anemometers and fluctuating environmental variables like solar irradiance and ambient temperature. Inconsistencies in maintaining authorized flow rates, as well as unaccounted-for heat losses, can have a substantial influence on the accuracy of thermal efficiency and energy performance evaluations.

This study's limitations include its dependence on controlled surroundings and specified climatic conditions, as well as its applicability limited to double-pass systems and low-temperature applications. The challenges include high production and material prices, the requirement for cost-benefit evaluations, market restrictions such as competition with traditional energy sources, and the need for commercialization-friendly regulations. Furthermore, although various configurations of hollow semi-stadium fins (HSSF) and baffles were examined, a more comprehensive examination of fin materials, as well as factors such as exergy efficiency and material durability, could yield additional insights. The following recommendations are suggested to improve future research and practical applications in light of the results of this study:

- Field-based experimental research is required to evaluate this novel solar air collector design under real-world circumstances and industry requirements. Further study should compare its performance to current designs in various operating scenarios and locations to determine its effectiveness and feasibility.
- Environmental assessment, life cycle cost analysis, and techno-economic analysis are crucial for assessing the sustainability and practicality of the solar collector system.
- Exergy studies and thermohydraulic studies are recommended to ensure a thorough assessment of the system's performance. Besides that, performing economic and environmental impact studies is essential to evaluate the viability and sustainability of the solar air collector utilizing multi-level HSSF and baffles.
- The use of various materials for the fins and baffles in future research could be investigated to enhance thermal efficiency.

CRediT authorship contribution statement

Muhammad Aqil Afham Rahmat: Writing – original draft, Methodology, Formal analysis, Conceptualization. Adnan Ibrahim: Supervision, Methodology, Funding acquisition, Conceptualization. Khaled M. Al-Aribe: Supervision, Methodology, Conceptualization. Muhammad Ubaidah Syafiq Bin Mustaffa: Supervision, Methodology. Ihsan Okta Harmailil: Writing – review & editing, Methodology. Sahibzada Imad Ud Din: Validation, Formal analysis.

Declaration of competing interest

The authors declare that they have no known competing financial interests or personal relationships that could have appeared to

influence the work reported in this paper.

Acknowledgement

Sincerely thank the Solar Thermal and Sustainable Technology Group, under Sustainable Resources, Nature and Smart Living Cluster, Kumpulan Penyelidikan Universiti (KPU) and Solar Energy Research Institute (SERI), Universiti Kebangsaan Malaysia, for their invaluable support and guidance throughout this project.

Data availability

Data will be made available on request.

References

- A. Borode, N. Ahmed, P. Olubambi, A review of solar collectors using carbon-based nanofluids, J. Clean. Prod. 241 (2019) 118311, https://doi.org/10.1016/j.iclenro.2019.118311
- [2] M.A. Afham Rahmat, et al., Revolutionizing drying chambers for sustainable energy technologies in food and agriculture: a comprehensive review, Sustain. Energy Technol. Assessments 75 (2025) 104205, https://doi.org/10.1016/j.seta.2025.104205.
- [3] A. Ahmad, O. Prakash, R. Kausher, G. Kumar, S. Pandey, S.M.M. Hasnain, Parabolic trough solar collectors: a sustainable and efficient energy source, Mater. Sci. Energy. Technol. 7 (2024) 99–106, https://doi.org/10.1016/j.mset.2023.08.002.
- [4] Á. Arroyo, N. Basurto, R. Casado-Vara, M. Timiraos, J.L. Calvo-Rolle, A Hybrid Intelligent modeling approach for predicting the solar thermal panel energy production, Neurocomputing 565 (2024) 126997, https://doi.org/10.1016/j.neucom.2023.126997.
- [5] F.B. Ismail, M.A.A. Rahmat, H.A. Kazem, A.S.M. Al-Obaidi, M.S. Ridwan, Maximizing energy via solar-powered smart irrigation: an approach utilizing a single-axis solar tracking mechanism, Irrig. Drain. (2024), https://doi.org/10.1002/ird.2937.
- [6] M.A.A. Rahmat, et al., An analysis of renewable energy technology integration investments in Malaysia using HOMER pro, Sustainability 14 (20) (2022), https://doi.org/10.3390/su142013684.
- [7] T. Ahmad, D. Zhang, A critical review of comparative global historical energy consumption and future demand: the story told so far, Energy Rep. 6 (2020) 1973–1991, https://doi.org/10.1016/j.egyr.2020.07.020.
- [8] D. Saygin, R. Kempener, N. Wagner, M. Ayuso, D. Gielen, The Implications for renewable energy innovation of doubling the share of renewables in the global energy mix between 2010 and 2030, Energies 8 (6) (2015) 5828–5865, https://doi.org/10.3390/en8065828.
- [9] N. Pongboriboon, V. Mariyappan, W. Wu, W. Chandra-Ambhorn, Economic and environmental analyses for achieving net-zero CO2 emissions of a green diesel production process, J. Taiwan Inst. Chem. Eng. 165 (2024) 105781, https://doi.org/10.1016/j.jtice.2024.105781.
- [10] A.G. Olabi, et al., Progress in Solar Thermal Systems and their Role in Achieving the Sustainable Development Goals, MDPI, Dec. 01, 2022, https://doi.org/10.3390/en15249501.
- [11] M.H. Machi, I. Farkas, J. Buzas, Enhancing thermal efficiency of double-pass solar air collectors: a comparative study on the role of V-angled perforated fins, Energy Rep. 12 (2024) 481–494, https://doi.org/10.1016/j.egyr.2024.06.048.
- [12] P. Dutta, P.P. Dutta, P. Kalita, Thermal performance study of a PV-driven innovative solar dryer with and without sensible heat storage for drying of Garcinia Pedunculata, Environ. Sci. Pollut. Control Ser. 31 (12) (2024) 18239–18259, https://doi.org/10.1007/s11356-023-27041-x.
- [13] P. Dutta, P.P. Dutta, P. Kalita, Energy and exergy study of a novel multi-mode solar dryer without and with sensible heat storage for Garcinia pedunculata, Energy Sources, Part A Recovery, Util. Environ. Eff. 45 (3) (Aug. 2023) 9266–9282, https://doi.org/10.1080/15567036.2023.2234325.
- [14] R.J. Barpatra Gohain, P.P. Dutta, N. Bora, Exergy, economic and environmental impacts analysis of a solar-biomass powered hybrid dryer for drying Eryngium Foetidum, Therm. Sci. Eng. Prog. 59 (2025) 103325, https://doi.org/10.1016/j.tsep.2025.103325.
- [15] H. Das, P. Dutta, P.P. Dutta, P.K. Choudhury, Experimental analysis of a solar air heater using waste mild steel chips as a sensible heat storage material, Environ. Sci. Pollut. Control Ser. (2024), https://doi.org/10.1007/s11356-024-35415-y.
- [16] P. Dutta, H. Das, P.P. Dutta, P. Kalita, Evaluation of an improved indirect solar dryer for Curcuma Amada without and with stone chips as thermal energy storage: an investigation on kinetics, energy, exergy, quality and economic aspects, J. Energy Storage 79 (2024) 110199, https://doi.org/10.1016/j.est.2023.110199.
- [17] M. Amir Aziat Bin Ishak, A. Ibrahim, K. Sopian, M. Faizal Fauzan, M. Aqil Afham Rahmat, A. Sufiyan Abd Hamid, Classification of Jet Impingement Solar Collectors-A Recent Development in Solar Energy Technology, 2023.
- [18] A. Fudholi, K. Sopian, A review of solar air flat plate collector for drying application, Renew. Sustain. Energy Rev. 102 (2019) 333–345, https://doi.org/10.1016/j.rser.2018.12.032.
- [19] N.I.S. Azha, H. Hussin, M.S. Nasif, T. Hussain, Thermal Performance Enhancement in Flat Plate Solar Collector Solar Water Heater: a Review, MDPI AG, Jul. 01, 2020, https://doi.org/10.3390/PR8070756.
- [20] N. Akram, et al., Experimental investigations of the performance of a flat-plate solar collector using carbon and metal oxides based nanofluids, Energy 227 (2021) 120452, https://doi.org/10.1016/j.energy.2021.120452.
- [21] S.I.U. Din, A. Ibrahim, R.K. Ajeel, A. Fazlizan, A.A. Ishak, A.B. Al-Aasam, Thermal performance analysis of a double-pass solar air heater with lava rock as porous and sensible heat storage material, J. Energy Storage 95 (Aug) (2024), https://doi.org/10.1016/j.est.2024.112564.
- [22] A.K. Bojarajan, et al., A holistic overview of sustainable energy technologies and thermal management in UAE: the path to net zero emissions, International J. Thermofluids 23 (2024) 100758, https://doi.org/10.1016/j.ijft.2024.100758.
- [23] K. Obaideen, et al., On the contribution of solar energy to sustainable developments goals: case study on Mohammed bin Rashid Al Maktoum Solar Park, International J. Thermofluids 12 (2021) 100123, https://doi.org/10.1016/j.ijft.2021.100123.
- [24] A. Kumar, A.K. Tiwari, Solar-assisted post-combustion carbon-capturing system retrofitted with coal-fired power plant towards net-zero future: a review, J. CO2 Util. 65 (2022) 102241, https://doi.org/10.1016/j.jcou.2022.102241.
- [25] B. Wang, Z.J. Ting, M. Zhao, Sustainable aviation fuels: key opportunities and challenges in lowering carbon emissions for aviation industry, Carbon Capture Sci. Technol. 13 (2024) 100263, https://doi.org/10.1016/j.ccst.2024.100263.
- [26] S.K.M. Balgehshiri, B. Zohuri, The impact of energy transition to net-zero emissions on the world economy and global strategies, J. Econ. Manag. Res. (4) (Aug. 2023) 1–7, https://doi.org/10.47363/JESMR/2023, 185.
- [27] E. Vengadesan, T. Arunkumar, T. Krishnamoorthi, S. Senthil, Thermal performance improvement in solar air heating: an absorber with continuous and discrete tubular and v-corrugated fins, Therm. Sci. Eng. Prog. 48 (2024) 102416, https://doi.org/10.1016/j.tsep.2024.102416.
- [28] J. Hu, G. Zhang, Performance improvement of solar air collector based on airflow reorganization: a review, Appl. Therm. Eng. 155 (2019) 592–611, https://doi.org/10.1016/j.applthermaleng.2019.04.021.
- [29] P.T. Saravanakumar, D. Somasundaram, M.M. Matheswaran, Thermal and thermo-hydraulic analysis of arc shaped rib roughened solar air heater integrated with fins and baffles, Sol. Energy 180 (2019) 360–371, https://doi.org/10.1016/j.solener.2019.01.036.
- [30] S. Chand, P. Chand, H. Kumar Ghritlahre, Thermal performance enhancement of solar air heater using louvered fins collector, Sol. Energy 239 (Jun. 2022) 10–24, https://doi.org/10.1016/j.solener.2022.04.046.

- [31] R. Biswas, P.P. Tripathy, Finite element based computational analysis to study the effects of baffle and fin on the performance assessment of solar collector, Therm. Sci. Eng. Prog. 49 (2024) 102431, https://doi.org/10.1016/j.tsep.2024.102431.
- [32] F. Chabane, N. Hatraf, N. Moummi, Experimental study of heat transfer coefficient with rectangular baffle fin of solar air heater, Front. Energy 8 (2) (2014) 160–172, https://doi.org/10.1007/s11708-014-0321-y.
- [33] T. Papingiotis, D.N. Korres, I. Koronaki, C. Tzivanidis, Energetical and exergetical analyses of a concentrating PV/T collector: a numerical approach, Appl. Sci. 13 (19) (Oct. 2023), https://doi.org/10.3390/app131910669.
- [34] H. Luqman Azeez, A. Ibrahim, B. Omer Ahmed, A.H.A. Al-Waeli, M. Jaber, M. Aqil Afham Rahmat, Energy and exergy analysis of a novel collector design in a photovoltaic thermal system: an experimental study, Appl. Therm. Eng. 256 (Nov) (2024), https://doi.org/10.1016/j.applthermaleng.2024.124125.
- [35] I. Ait Laasri, M. Charai, M.O. Mghazli, A. Outzourhit, Energy performance assessment of a novel enhanced solar thermal system with topology optimized latent heat thermal energy storage unit for domestic water heating, Renew. Energy 224 (Apr) (2024), https://doi.org/10.1016/j.renene.2024.120189.
- [36] P. Rani, P.P. Tripathy, Experimental investigation on heat transfer performance of solar collector with baffles and semicircular loops fins under varied air mass flow rates, Int. J. Therm. Sci. 178 (2022) 107597, https://doi.org/10.1016/j.ijthermalsci.2022.107597.
- [37] H.E. Ahmed, Optimization of thermal design of ribbed flat-plate fin heat sink, Appl. Therm. Eng. 102 (2016) 1422–1432, https://doi.org/10.1016/j.applthermaleng.2016.03.119.
- [38] G.W. Mann, S. Eckels, Multi-objective heat transfer optimization of 2D helical micro-fins using NSGA-II, Int. J. Heat Mass Tran. 132 (2019) 1250–1261, https://doi.org/10.1016/j.ijheatmasstransfer.2018.12.078.
- [39] H.P. Garg, A.R. Shukla, R.C. Agnihotri, S. Chakravertty, Development of a Simple Low-Cost Solar Simulator for Indoor Collector Testing, 1985.
- [40] H. Jarimi, M.N. Abu Bakar, M. Othman, M.H. Din, Bi-fluid photovoltaic/thermal (PV/T) solar collector: experimental validation of a 2-D theoretical model, Renew. Energy 85 (2016) 1052–1067, https://doi.org/10.1016/j.renene.2015.07.014.
- [41] A. Fudholi, K. Sopian, M.Y. Othman, M.H. Ruslan, B. Bakhtyar, Energy analysis and improvement potential of finned double-pass solar collector, Energy Convers. Manag. 75 (2013) 234–240, https://doi.org/10.1016/j.enconman.2013.06.021.
- [42] A.Y. Al-Ahmad, et al., Modular LED arrays for large area solar simulation, Prog. Photovoltaics Res. Appl. 27 (2) (Feb. 2019) 179–189, https://doi.org/10.1002/pip.3072.
- [43] M.A.A. Bin Ishak, A. Ibrahim, A. Fazlizan, M.F. Fauzan, K. Sopian, A.A. Rahmat, Exergy performance of a reversed circular flow jet impingement bifacial photovoltaic thermal (PVT) solar collector, Case Stud. Therm. Eng. 49 (2023) 103322, https://doi.org/10.1016/j.csite.2023.103322.
- [44] S.D. Prasetyo, et al., Optimization of photovoltaic thermal collectors using fins: a review of strategies for enhanced solar energy harvesting, Math. Model. Eng. Probl. 10 (4) (Aug. 2023) 1235–1248, https://doi.org/10.18280/mmep.100416.
- [45] J.A. Duffie, W.A. Beckman, Solar Engineering of Thermal Processes, Wiley, 2013.
- [46] A.B. Al-Aasam, A. Ibrahim, K. Sopian, B. Abdulsahib M, M. Dayer, Nanofluid-based photovoltaic thermal solar collector with nanoparticle-enhanced phase change material (Nano-PCM) and twisted absorber tubes, Case Stud. Therm. Eng. 49 (2023) 103299, https://doi.org/10.1016/j.csite.2023.103299.
- [47] S. Imad Ud Din, A. Ibrahim, A. Fazlizan, M.A.A. Ishak, A.S. Abd Hamid, Performance analysis of a novel photovoltaic thermal PVT double pass solar air heater with cylindrical PCM capsules using CFD, Int. J. Renew. Energy Resour. 13 (Sep) (2023), https://doi.org/10.20508/ijrer.v13i3.14136.g8814.
- [48] F. Jafarkazemi, E. Ahmadifard, Energetic and exergetic evaluation of flat plate solar collectors, Renew. Energy 56 (2013) 55–63, https://doi.org/10.1016/j.renene.2012.10.031.
- [49] T. Merembayev, Y. Amirgaliyev, M. Kunelbayev, D. Yedilkhan, Thermal loss analysis of a flat plate solar collector using numerical simulation, Comput. Mater. Continua (CMC) 73 (3) (2022) 4627–4640, https://doi.org/10.32604/cmc.2022.027180.
- [50] L. Shui-lian, M. Xiang-rui, W. Xin-li, Heat transfer and friction factor correlations for solar air collectors with hemispherical protrusion artificial roughness on the absorber plate, Sol. Energy 118 (2015) 460–468, https://doi.org/10.1016/j.solener.2015.05.047.
- [51] A.F. Ismail, A.S.A. Hamid, A. Ibrahim, H. Jarimi, K. Sopian, Performance analysis of a double pass solar air thermal collector with porous media using lava rock, Energies 15 (3) (Feb. 2022), https://doi.org/10.3390/en15030905.
- [52] R.K. Ajeel, S.N. Fayyadh, A. Ibrahim, S.M. Sultan, T. Najeh, Comprehensive analysis of heat transfer and pressure drop in square multiple impingement jets employing innovative hybrid nanofluids, Res. Eng. 21 (2024) 101858, https://doi.org/10.1016/j.rineng.2024.101858.
- [53] M.A.M. Daza-Gómez, C.A. Gómez Velasco, J.C. Gómez Daza, N. Ratkovich, 3D computational fluid dynamics analysis of a convective drying chamber, Processes 10 (12) (Dec. 2022), https://doi.org/10.3390/pr10122721.
- [54] H.A. mohammed Hussein, R. Zulkifli, W.M.F. Bin Wan Mahmood, R.K. Ajeel, Numerical investigation and parameter analysis of oblique-finned with square corrugations to improve heat transfer performance, Alex. Eng. J. 76 (2023) 669–688, https://doi.org/10.1016/j.aej.2023.06.051.
- [55] N.I. Román-Roldán, J.F. Ituna Yudonago, A. López-Ortiz, J. Rodríguez-Ramírez, S. Sandoval-Torres, A new air recirculation system for homogeneous solar drying: computational fluid dynamics approach, Renew. Energy 179 (2021) 1727–1741, https://doi.org/10.1016/j.renene.2021.07.134.
- [56] G. Barone, A. Buonomano, S. Kalogirou, P. Ktistis, A. Palombo, A holistic methodology for designing novel flat plate evacuated solar thermal collectors: modelling and experimental assessment, Renew. Energy 232 (2024) 120967, https://doi.org/10.1016/j.renene.2024.120967.
- [57] R.A.M. Coetzee, A. Mwesigye, Z. Huan, A numerical analysis and optimization of the dynamic performance of a multipurpose solar thermal system for residential applications, Sci. Technol. Built. Environ. 24 (10) (Nov. 2018) 1156–1173, https://doi.org/10.1080/23744731.2018.1479593.
- [58] C.T. Simeu, D. Njomo, V.S. Chara-Dackou, M.H. Babikir, Comparative study of thermal performance improvement of parabolic trough solar collector using different heat transfer fluids, economic and environmental analysis of power generation, Res. Eng. 23 (2024) 102353, https://doi.org/10.1016/j. pp. 2024.102353
- [59] S. Şevik, M. Abuşka, Thermal performance of flexible air duct using a new absorber construction in a solar air collector, Appl. Therm. Eng. 146 (2019) 123–134, https://doi.org/10.1016/j.applthermaleng.2018.09.100.
- [60] N.J. Yusaidi, M.F. Fauzan, A.F. Abdullah, A. Ibrahim, A.A. Ishak, Theoretical and experimental investigations on the effect of double pass solar air heater with staggered-diamond shaped fins arrangement, Case Stud. Therm. Eng. 60 (2024) 104619, https://doi.org/10.1016/j.csite.2024.104619.
- [61] A. Daliran, Y. Ajabshirchi, Theoretical and experimental research on effect of fins attachment on operating parameters and thermal efficiency of solar air collector, Inform. Proces. Agri. 5 (4) (2018) 411–421, https://doi.org/10.1016/j.inpa.2018.07.004.
- [62] H. Farzan, A. Iranmanesh, A. Mohsenifard, Investigation on different cooling strategies for photovoltaic thermal Systems: an experimental study, Appl. Therm. Eng. 250 (2024) 123537, https://doi.org/10.1016/j.applthermaleng.2024.123537.
- [63] A. Thakur, et al., Improved performance evaluation of a dual passage solar thermal collector using staggered turbulators, Therm. Sci. Eng. Prog. 53 (2024) 102668, https://doi.org/10.1016/j.tsep.2024.102668.
- [64] M.A. Kherrafi, et al., Performance enhancement of indirect solar dryer with offset strip fins: experimental investigation and comparative analysis, Sol. Energy 266 (2023) 112158, https://doi.org/10.1016/j.solener.2023.112158.
- [65] P. Dutta, P.P. Dutta, P. Kalita, Thermal performance studies for drying of Garcinia pedunculata in a free convection corrugated type of solar dryer, Renew. Energy 163 (2021) 599–612, https://doi.org/10.1016/j.renene.2020.08.118.